ウェブサイト公開用

海外特別研究員最終報告書

独立行政法人　日本学術振興会　理事長　殿

採用年度　平成３１年
受付番号　２０１９６０２９７
氏　　名　岩本　紘明

（氏名は必ず自署すること）

海外特別研究員としての派遣期間を終了しましたので、下記のとおり報告いたします。
なお、下記及び別紙記載の内容については相違ありません。

記

1. 用務地（派遣先国名）用務地：　ケンブリッジ大学　　　　　（国名：　英国　　　　　　　）

2. 研究課題名（和文）※研究課題名は申請時のものと違わないように記載すること。
　　複雑有機分子に対する高選択的 C(sp3)−H 結合変換反応の理論的設計

3. 派遣期間：平成　３１年　４月　１日　〜　令和　元年　９月　１２日

4. 受入機関名及び部局名
　　ケンブリッジ大学化学科

5. 所期の目的の遂行状況及び成果…書式任意　　**書式任意（A4 判相当３ページ以上、英語で記入も可）**
　（研究・調査実施状況及びその成果の発表・関係学会への参加状況等）
　（注）「6. 研究発表」以降については様式 10−別紙１〜４に記入の上、併せて提出すること。

Background:

　Methylated nucleotides such as *N*-methyl adenine (N6mA) and 5-methyl cytosine (5mC) in DNA have been found to profoundly relative to various genetical events such as transcription and embryogenesis without changing its sequence. Nowadays, many types of modified nucleotides have been found from genomes of eukaryotes and prokaryotes. Therefore, various methods for DNA sequencing have been developed to reveal where the modified nucleotides are located in DNA sequence because their epigenetic behavior are important for understanding biological events and genetic engineering.

　Our group have developed the N-methylated adenine (N6mA) selective DNA modification via C(sp³)–H activation by photoredox catalyst (Figure 1). The reaction of the DNA oligomer containing N6mA with photocatalyst [Ru(phen)₃]²⁺, quinuclidine and 3-nitropyridine derivative under photoirradiation conditions gave the *N*-hydroxy formamidine structure bearing a pyridine ring to N6mA in the DNA oligomer. Therefore, the 3-nitropyridine baring a functional group such as a terminal alkyne moiety can be used as a probe for the N6mA selective detection through pull-down assay.
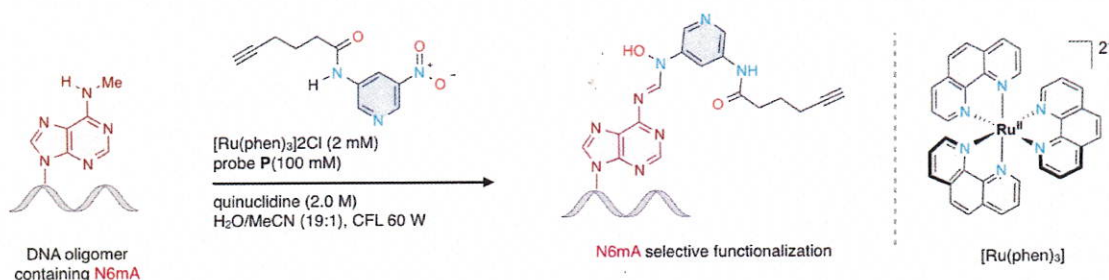

Figure 1. Proposed reaction pathway for N-methyl selective functionalization of adenine (N6mA).

The plausible reaction pathway of N6mA selective functionalization was shown in Figure 1. This N6mA selective DNA modification includes three redox cycle at least because the N6mA loses two hydrogen atoms and the nitropyridine also loses one oxygen atom. The first redox process is a hydrogen atom transfer (HAT) between N6mA and a quinuclidine radical cation generated by oxidation with photocatalyst. This process provides the α-amino radical **I** and a nitropyridine radical anion. The second redox process is an oxygen abstract from the nitropyridine radical anion by a quinuclidine radical cation. This process provides a nitrosopyridine and a quinuclidine N-oxide which has been detected by LC-MS. And then, the coupling reaction between the α-amino radical **I** and the nitrosopyridine gives the corresponding aminal **II** bearing a N-oxide moiety. The third redox process is a HAT between **II** and quinuclidine radical cation to give the corresponding N-hydroxy formamidine **V**.
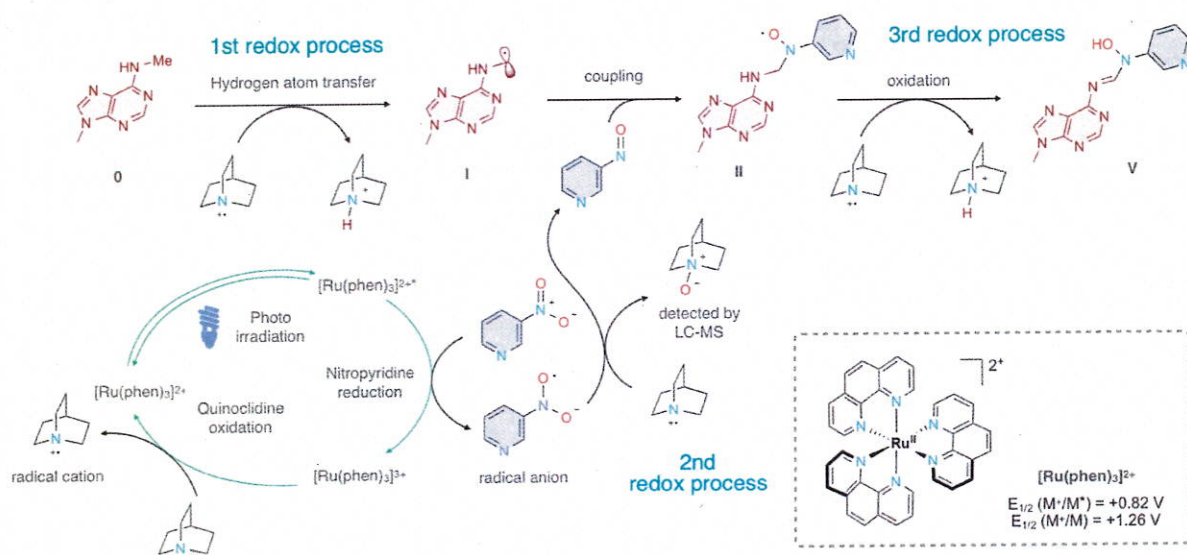

Figure 2. Proposed reaction pathway for N-methyl selective functionalization of adenine (N6mA).

Part 1. DFT Calculation of reaction pathway of *N*-methyl adenine (N6mA) functionalization

At first, the hydrogen atom transfer (HAT) step between N6mA and quinuclidine radical cation was investigated by the density functional theory (DFT) calculation (Figure 1-1). The activation energy barrier of this HAT was reasonable to proceed at room temperature ($\Delta G^{\ddagger}$ = +17.0 kcal/mol). And this HAT was slightly exothermic process (ΔG = −3.2 kcal/mol). Furthermore, the calculated bond dissociation energy (BDE) of N6mA was lower than the reported value of the protonated quinuclidine cation [$BDE_{(C-H)}$: 93.4 kcal/mol (DFT); $BDE_{(N-H)}$: 100 kcal/mol (reported)].
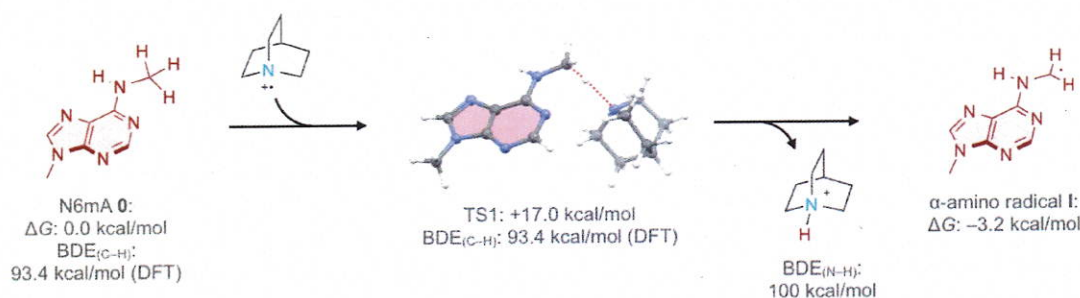

Figure 1-1. Transition state (TS1) of hydrogen atom transfer (HAT) between N6mA and quinuclidine radical cation at CAM-B3LYP-D3(BJ)/6-311++(2df,2p)/SMD(water)//CAM-B3LYP/6-31+(d,p) 298K level of theory.

Next, the radical coupling step between the α-amino radical **I** and 3-nitrosopyridine was calculated (Figure 1-2). It has been known that the carbon radical and nitroso compound react at a nitrogen atom of the nitroso moiety to form a new carbon–nitrogen bond. In 2015, Alaniz and co-workers reported the copper(I)-catalyzed amination of α-haloesters using nitroso compounds through the α-keto radicals (Figure 1-2a). To confirm the reaction mechanism of this α-amination reaction, the DFT calculation of the transition state of the radical addition step (**TS**-N or **TS**-O) was carried out. The transition state of C–N bond formation by α-keto radical **I** and nitrosobenzene (**TS**-N) was more favorable than that of C–O bond (**TS**-O) (**TS**-N: $\Delta G^{\ddagger}$ = +6.0 kcal/mol; **TS**-O: $\Delta G^{\ddagger}$ = +9.3 kcal/mol; $\Delta\Delta G^{\ddagger}$ = +3.3 kcal/mol).

This indicated that the N-adduct product was only obtained from this reaction system. Contrary, in the case of α-amino radical, the activation energy of transition state (**TS2**-O) which is a reaction at an oxygen atom of the nitroso moiety was more favorable compared to that of the transition state (**TS2**-N) which is a reaction at a nitrogen atoms (Figure 1-2b, **TS2**-O: $\Delta G^{\ddagger}$ = +5.0 kcal/mol; **TS2**-N: $\Delta G^{\ddagger}$ = +7.4 kcal/mol; $\Delta\Delta G^{\ddagger}$ = +2.4 kcal/mol). Whereas, the thermodynamic stability of the radical adducts indicated that the *N*-addition product **III**-N was highly stabilized compared to the *O*-addition product **III**-O in both cases. However, in the view of reaction reversibility, these radical addition process should be controlled kinetically.
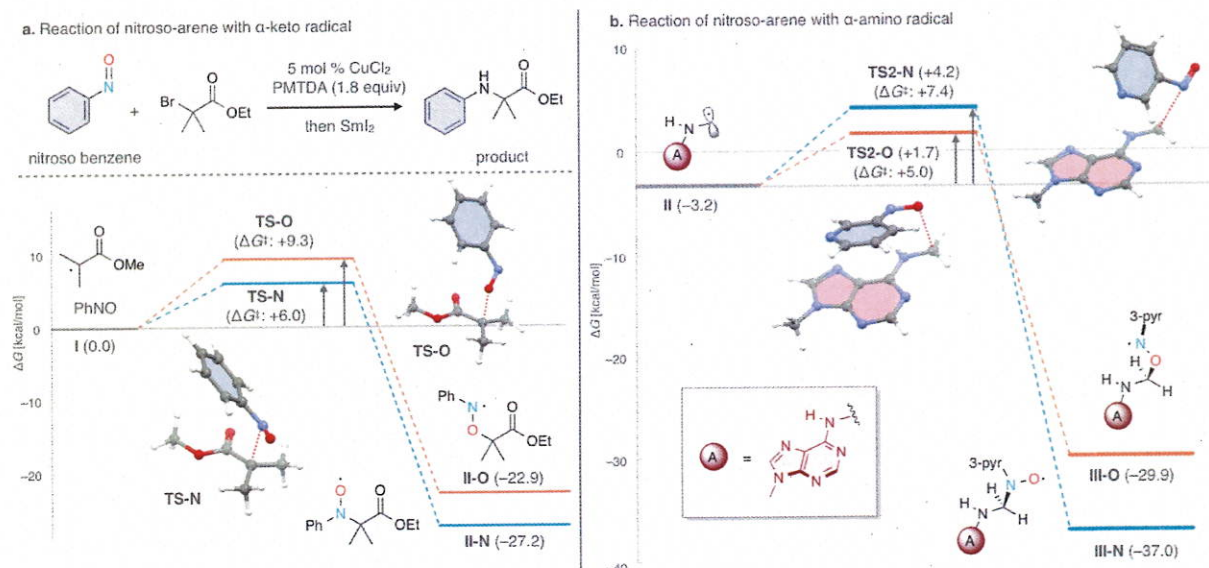

Figure 1-2. Transition state of radical coupling between carbon radical and nitroso compound. **a.** Coupling of α-keto radical **I** and nitrosobenzene (TS) reported by Alaniz and co-workers. **b.** Coupling of α-amino radical **II** and 3-nitrosopyridine (TS2). All calculation was conducted at CAM-B3LYP-D3(BJ)/6-311++(2df,2p)/SMD(water)//CAM-B3LYP/6-31+(d,p) 298K level of theory.

To reveal the inversed reaction selective, the detailed analysis of the characters of α-amino radicals was conducted (Figure 1-3). The Muliken charge and spin distribution of the transition state structures was calculated to explain the radical species depended reaction selectivity. The α-keto radical should be an electrophilic radical and α-amino radical should be a nucleophilic radical because the spin localized carbon of α-keto radical was positive (**TS**-O: charge/spin: +0.67/−0.47; **TS**-N: charge/spin: +0.84/−0.55), in contrast, the spin localized carbon of α-amino radical was negative (**TS2**-O: charge/spin: −0.36/+0.64; **TS2**-N: charge/spin: −0.54/+0.83). Therefore, the nucleophilicity of a spin localized carbon would control the regioselectivity of radical addition to nitroso compounds.
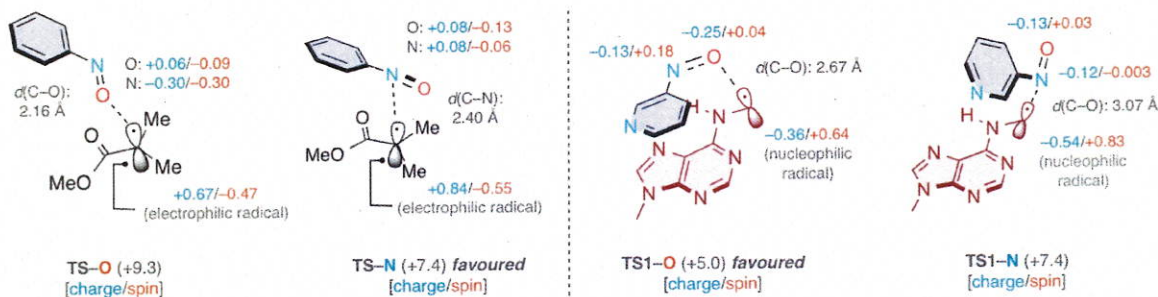

Figure 1-3. Detailed analysis of transition states of radical coupling between carbon radical and nitroso compound.

Although the computational study proposed the O-selective coupling of α-amino radical **II** with 3-nitrosopyridine, the detected coupling product **V** contained a C–N bond (Figure 2). Thus, it was expected that the rearrangement pathway from C–O bond to C–N bond during the third redox process of **III**-O would exist. The DFT calculation suggested that second HAT between **III**-O and quinuclidine radical cation (**TS3**-O) followed by formation of an oxaziridine **IV**-O and a C–O bond cleavage would be a possible pathway to **V** from **III**-O (Figure 1-4). At first, the activation energy barrier **TS3**-O [singlet] of the second HAT between **II**-O and quinuclidine radical cation was higher than that of first HAT (**TS1**). However, the activation energy of **TS3**-O [singlet] was reasonable to proceed at room temperature ($\Delta G^{\ddagger}$ = +21.3 kcal/mol). Furthermore, the intermediate **III**-O showed non-radical character

because the singlet biradical structure would significantly be unstable compared to the closed shell structure **III**-O. Subsequently, the cyclization of the zwitterionic species **III**-O to give the oxaziridine **IV**-O via **TS4**-O also displayed the reasonable activation energy barrier ($\Delta G^{\ddagger}$ = +11.0 kcal/mol). Finally, the ring opening C–O bond cleavage triggered by the deprotonation of the amine moiety of adenine would furnish the corresponding N-hydroxy formamidine **V** through a low transition state **TS5**-O ($\Delta G^{\ddagger}$ = +2.8 kcal/mol).
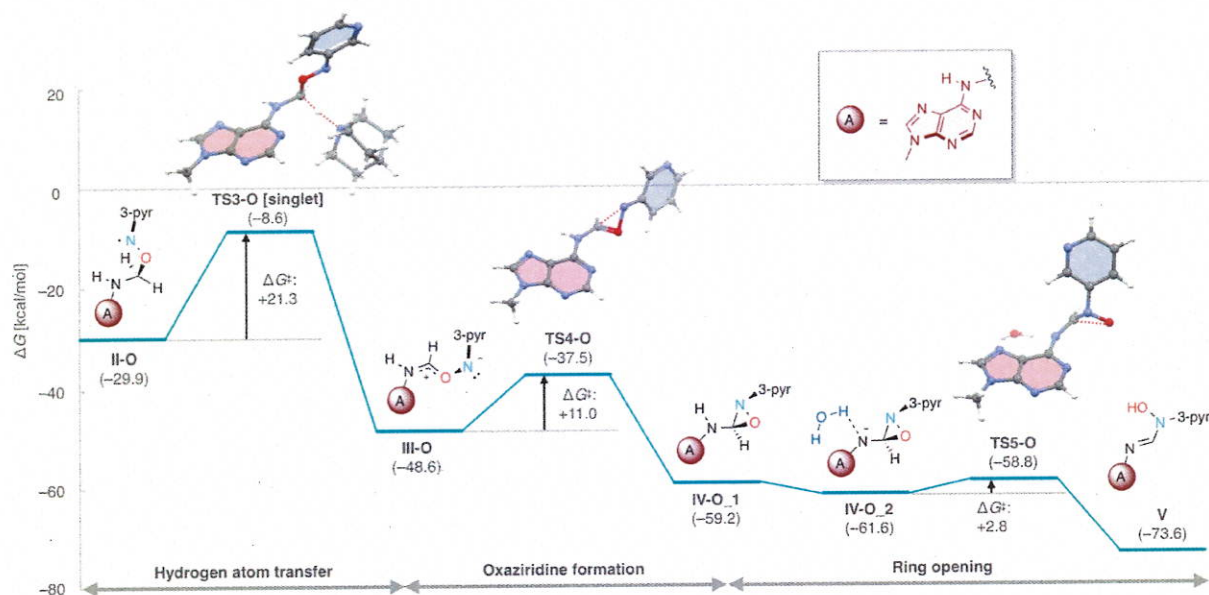

Figure 1-4. Energetic analysis of proposed reaction pathway to **V** from III-O through C–N formation and C–O bond cleavage at CAM-B3LYP-D3(BJ)/6-311++(2df,2p)/SMD(water)//CAM-B3LYP/6-31+(d,p) 298K level of theory.

Finally, a summary of energetic analysis of the N6mA functionalization by DFT calculation was shown in Figure 1-5. Basically, the functionalization was downhill-type pathway. The reaction pathway was branched at the radical addition into C–N bond formation or C–O bond formation pathway. The DFT calculation study indicated the C–O bond formation would prefer to the C–N bond formation in the radical coupling step (TS2). However, as mentioned above, the reaction pathway from the C–O coupling intermediate **II**-O to *N*-hydroxy formamidine **V** was highly complicated. On the other hand, the reaction pathway via the C–N coupling intermediate **II**-N to **V** was simpler than the pathway from **III**-O. Furthermore, the calculated activation energy of the HAT between **II**-N and quinuclidine radical cation was lower than that of the pathway via **II**-O (**TS3**-O: $\Delta G^{\ddagger}$ = +21.3 kcal/mol; **TS3**-N: $\Delta G^{\ddagger}$ = +14.0 kcal/mol). Therefore, the other reaction pathways might potentially be hidden in the pathway from **II**-O because the other possible pathways for any side products were not considered in this DFT calculation of the reaction pathway.
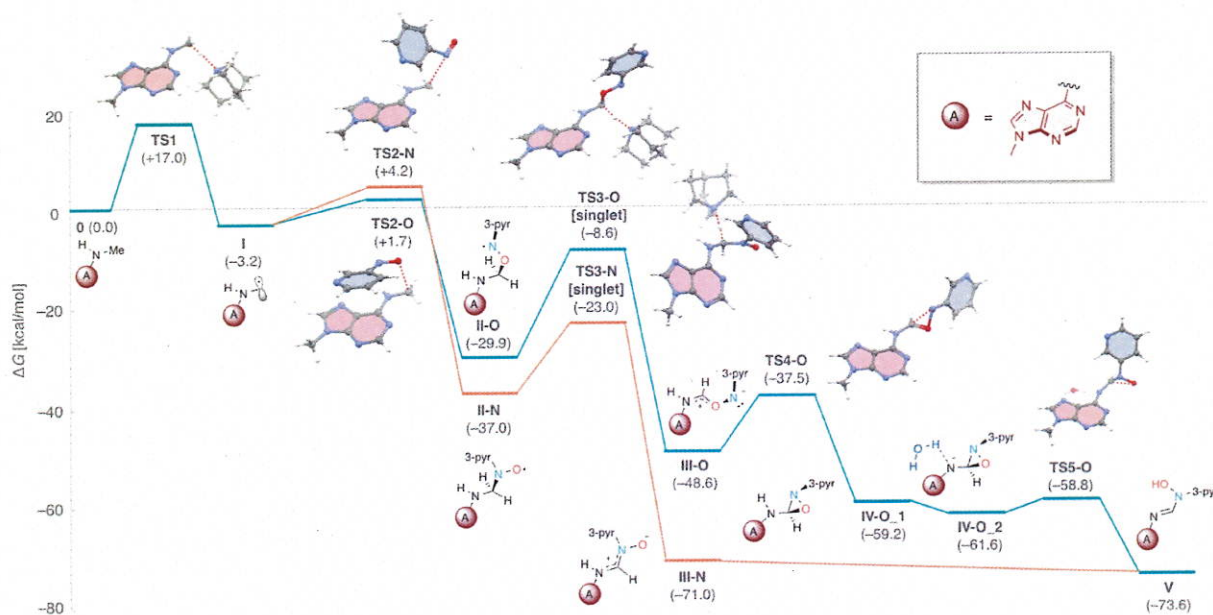

Figure 1-5. Energetic analysis of proposed reaction pathway to **V** from III-O through C–N formation and C–O bond cleavage at CAM-B3LYP-D3(BJ)/6-311++(2df,2p)/SMD(water)//CAM-B3LYP/6-31+(d,p) 298K level of theory.

Part 2. DFT Calculation of reaction pathway of *N*-methyl adenine (N6mA) functionalization

In this part, the redox potential-depended reaction efficiency and selectivity of *N*-methyl selective modification of DNA containing N6mA was investigated to improve the reaction efficiency and reveal the origin of reaction selectivity. Reduction potentials of organic compounds are significantly important factors for development of photoredox reactions. Although the redox potentials of photoredox catalysts have been reported, the redox potentials of many organic molecules have not experimentally been measured.

In this work, at first, the reduction step of nitroarene compounds by [Ru(II)] was focused on, because the nitroarene is a key compound for this modification system (Figure 2-1). Therefore, it was hypothesized that the nitropyridine showing higher redox potential should enhance the reactivity of this photoredox catalyst process. Although the redox potentials of [Ru(phen)₃]²⁺ complex [$E_{1/2}$ (M⁺/M*) = −0.87 V, $E_{1/2}$ (M⁺/M) = +1.26 V], the potentials of almost all nitroarenes have been unreported. Therefore, the prediction of redox potential of nitro-pyridine derivatives using density functional theory (DFT) calculation was carried out. The computational estimation of redox potential would allow to obtain the corresponding redox potential readily. Furthermore, the design of new nitroarene exhibiting higher reactivity based on the predicted redox potential was also anticipated.
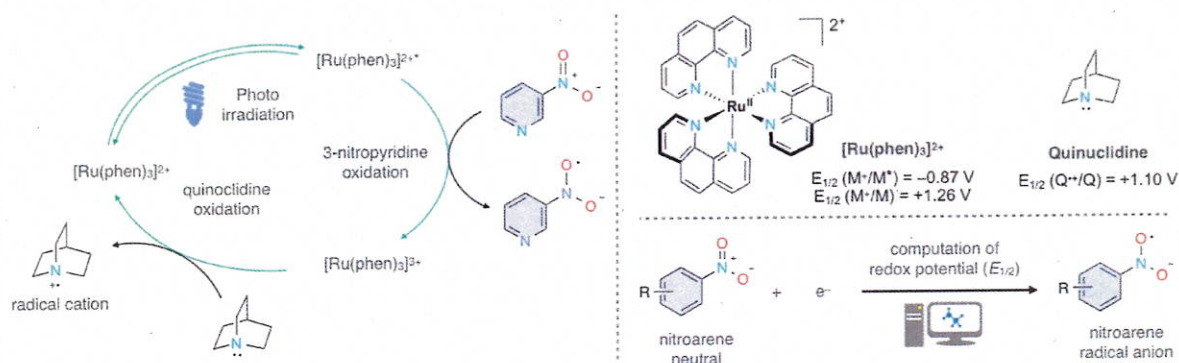

Figure 2-1. Proposed redox cycle of [Ru(phen)₃]²⁺ with quinuclidine and 3-nitropyridine and redox potentials.
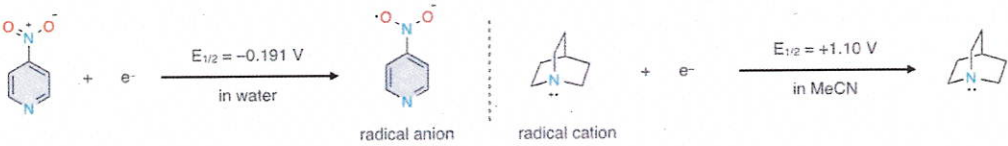
The calculated redox potential ($E_{1/2}^{0,calc}$) can be obtained from equation (1) where $\Delta G_{1/2}^{0,calc}$ is difference of standard Gibbs energy of formation between the oxidation state and reduction state, n_e is a number of electron involving redox process and F is Faraday constant. The standard Gibbs energy $\Delta G_{1/2}^{0,calc}$ can be obtained from the corresponding DFT calculation. In the case of the calculation of redox potential against standard hydrogen electrode (SHE), the value has to be corrected by $E_{1/2}^{0,SHE} = 4.281$ V. Furthermore, in the case of the potential against standard calomel electrode, the value has to be corrected by $E_{1/2}^{0,SCE}$.

$$E_{1/2}^{0,calc} = -\frac{\Delta G_{1/2}^{0,calc}}{n_e F} - E_{1/2}^{0,ref} \qquad (1)$$
$$E_{1/2}^{0,SHE} = 4.281 \text{ V}$$
$$E_{1/2}^{0,SCE} = E_{1/2}^{0,SHE} + 0.141 \text{ V}$$

Next, the screening of DFT calculation method was conducted to find a high accurate method for the redox potential prediction by the comparison between the reported values and calculated values (Table 2-1). The reductions of 4-nitro-pyridine and quinuclidine were employed as reference because these experimental redox potentials have been reported. According to other papers regarding to DFT calculation of organic radical species, CAM-B3LYP method often gives high accurate results. In our case, this CAM-B3LYP also showed higher accuracy than the other method M06-2X and B3LYP. Whereas, the basis set of calculation was also important for accuracy. The use of def2-SVP was not better than 6-31+G(d,p) for the calculation of 4-nitro-pyridine. That the accurate calculation of anion state often requires a diffuse function in the basis set, but def2-SVP does not include a diffuse function. The lack of a diffuse function in the basis set would be reason why the def2-SVP showed low accuracy. The accuracy between the corresponding double zeta and triple zeta basis set was almost same. Therefore, in this study, the double zeta basis set 6-31+G(d,p) was used because of the calculation cost.

Table 1. Screening of calculation method for high accuracy

calculation method	4-nitro-pyridine (in water)		Quinuclidine (in MeCN)	
	E (V)	error (V)	E (V)	error (V)
experimental	-0.191	-	+1.10	-
M06-2X/6-31+G(d,p)/SMD	-0.309	-0.118	N.A.	N.A.
B3LYP/6-31+G(d,p)/SMD	-0.288	-0.097	+0.688	-0.412
CAM-B3LYP/6-31+G(d,p)/SMD	-0.198	-0.007	+0.770	-0.33
CAM-B3LYP/6-311+G(d,p)/SMD	-0.135	0.056	+0.836	-0.26
CAM-B3LYP/def2-SVP/SMD	-0.762	-0.571	+0.732	-0.37

The highly accurate calculation method in hand, the exhaustive screening of redox potentials of more than 40 nitroarenes was carried out (Figure 2-2). This computational screening targeted not only nitropyridine derivatives but also other nitroarenes. However, the screening results indicated that nitropyridines basically shows higher redox potential than those of nitroarenes such as nitrobenzene and nitroindoles. The position of a nitro group on the pyridine ring had an impact on the redox potential. 4-nitropyridines showed higher redox potentials than 2- or 3-nitropyridines. Furthermore, the substituents on the pyridine ring exerted an influence on the redox potentials. The redox potential of a 3-nitropyridine derivative bearing a week electron-donating amide moiety on 5 position (3-nitro-5-N-Ac pyridine) was similar to that of 3-nitropyrisine (−0.33 V). Whereas, a 3-nitropyridine derivative bearing an electron-withdrawing group on 6-position (3-nitro-6-CONHMe-pyridine) showed higher redox potential than those of the other 3-nitropyridine derivatives (−0.22 V). Furthermore, 4-nitropyridine derivatives basically showed high redox potential (> −0.20 V). In particular, the 4-nitropyridine derivatives bearing an electron-withdrawing group displayed significantly higher redox potential (> −0.13 V). Therefore, it was expected that these 4-nitropydirine would improve the reactivity for the N6mA selective DNA modification.
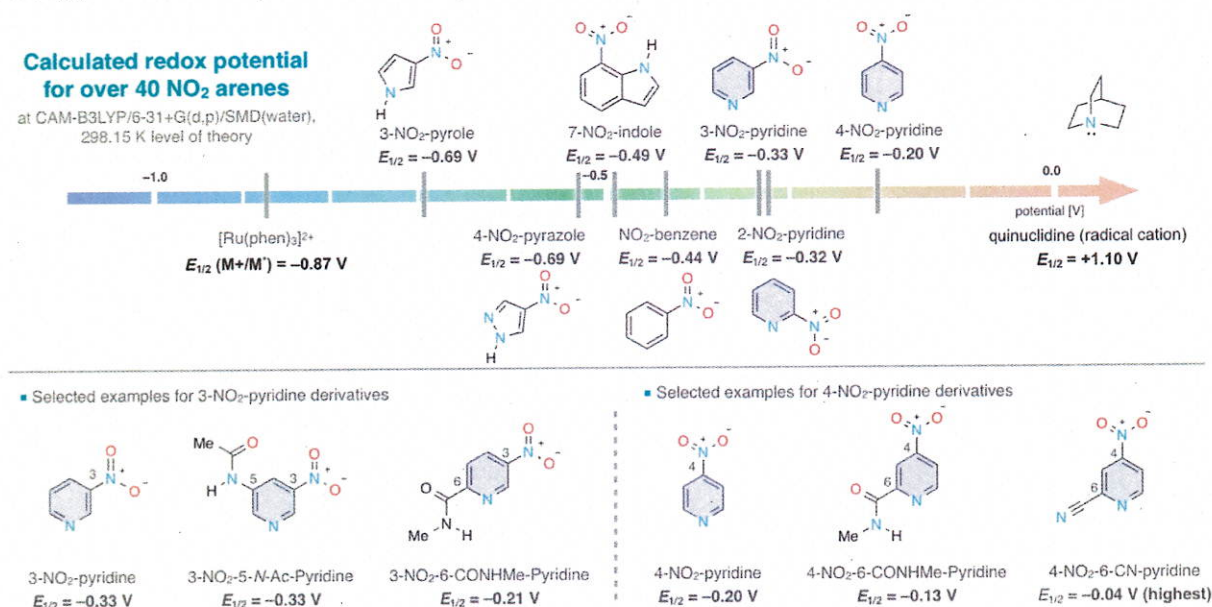
Figure 2-2. Redoxpotential index of nitroarene derivatives by DFT calculation at CAM-B3LYP/6-31+G(d,p)/SMD (water) at 298 K level of theory.

The 4-nitropyridine derivatives showing high redox potential were tested to the reactions of the DNA oligomer including a N6mA (Figure 2-3). The modification using 4-nitropyridine bearing an amide moiety at 6-position 4-NO₂-6-CONHMe-pyridine resulted in high conversion. However, the only corresponding demethylated DNA oligomer was obtained. Furthermore, the 4-nitropyridine bearing a nitrile group at 6-position 4-NO₂-6-CN-pyridine showed moderate conversion because the nitrile group would be reactive under photoirradiation conditions. Therefore, highly oxidative nitro compounds toward the photocatalyst would enhance the reactivity. However, the reaction

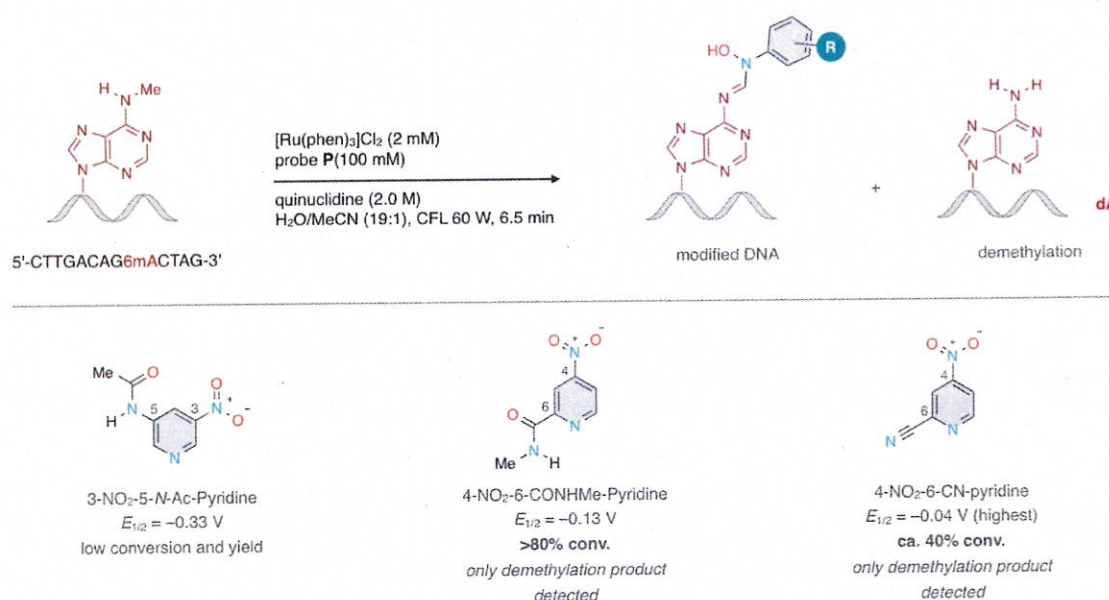selectivity between the N-methyl selective functionalization and the demethylation was inversed.

Figure 2-3. Experimental evaluation of 4-nitropyridine derivatives bearing an electron-withdrawing group.

The detail of the reaction between the α-amino radical species ([6-CH$_2$-A]•) and nitrosopyridines was investigated to discuss the reaction selectivity depending on nitropyridine (Figure 2-4). It was speculated that the single electron transfer (SET) between N6mA radical and 3-nitrosopyridine would be the key of the reaction selectivity because iminium cation should be unstable under basic aqueous conditions (Figure 2-4a). In the case of 3-nitro-pyridine, the calculated redox potentials of the N6mA iminium cation and 3-nitrosopyridine were almost same (6-CH$_2$-A: $E_{1/2}$ = −0.23 V, 3-nitrosopyridine: $E_{1/2}$ = −0.22 V). Furthermore, the thermodynamic stability of N6mA radical species and 3-nitrosopyridine indicated that this SET should be an endothermic process. ($\Delta\Delta G$ = +1.3 kcal/mol). Contrary, in the case of the 4-nitrosopyridine bearing an amide moiety, the redox potential was sufficiently higher than those of N6mA iminium cation ($E_{1/2}$ = +0.05 V). Moreover, the DFT study suggested that the SET between the α-amino radical and 4-nitroso derivative should be an exothermic process. Therefore, the redox potential of nitroso compounds would be important for the reaction selectivity for the N6mA selective DNA modification with a nitropyridine probe by photoredox catalyst as well as the redox potential of nitro compounds. The redox potential index of nitro- and nitrosopyridine suggested that the 4-nitropydine bearing an amide moiety can also oxidize the α-amino radical to the iminium cation due to its high redox potential ($E_{1/2}$ = −0.13) (Figure 2-4b).
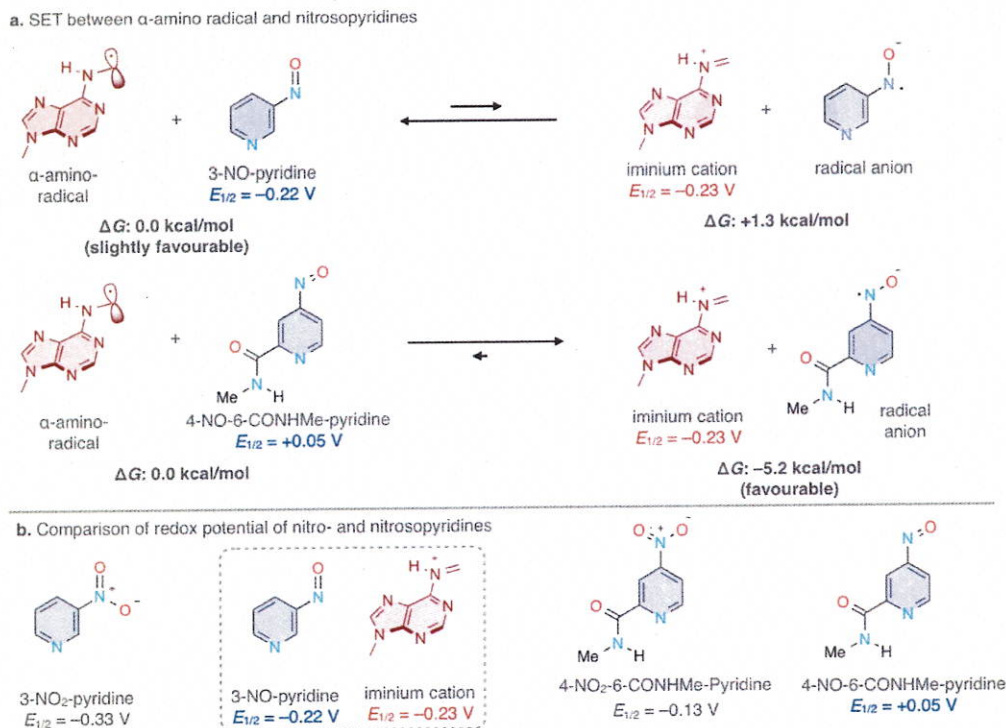
Figure 2-4. a. Energetic analysis of SET between α-amino radical and nitroso compounds at Redox potentials of nitro-pyridine derivatives and Adenine at CAM-B3LYP-D3(BJ)/6-311++(2df,2p)/SMD(water)//CAM-B3LYP/6-31+(d,p) 298K level of theory. **b.** redox potential: CAM-B3LYP/6-31+G(d,p)/SMD (water) at 298 K level of theory;

The mechanistic study using DFT calculation indicated the high redox potential of nitroso compounds would accelerate the SET as a side reaction to demethylation. And then, the exhaustive screening of redox potentials of nitroso compounds was conducted. In this screening, the nitroso compounds which show redox potential higher than −0.33 V in the corresponding nitro compound from were targeted. The screening result was plotted in Figure 2-5. The plot displayed that the redox potentials of nitrosopyridines relatively higher than those of other nitroarenes (yellow dots). The 4-nitro or nitrosopyrimidine derivatives also showed high redox potentials (green dots) deriInterestingly, the redox potentials of nitroso-furans or thiophenes were relatively low (blue and gray dots). Furthermore, the screening data was filtered by the redox potentials of nitro- and nitrosoarenes less than −0.23 V (yellow area). Then, the following four nitroarenes satisfying the requirement were found: 1) 3-nitro-6-NAc-pyridine (NO$_2$: $E_{1/2}$ = −0.33; NO: $E_{1/2}$ = −0.31), 2) 2-MeO-5-nitropyrimidine (NO$_2$: $E_{1/2}$ = −0.33; NO: $E_{1/2}$ = −0.26), 3) 2- nitrofuran (NO$_2$: $E_{1/2}$ = −0.31; NO: $E_{1/2}$ = −0.31), 4) 2-nitrothiophene (NO$_2$: $E_{1/2}$ = −0.32; NO: $E_{1/2}$ = −0.29). These nitro- or nitrosoarenes were predicted as higher reactive and selective probes for the N6mA selective DNA modification.
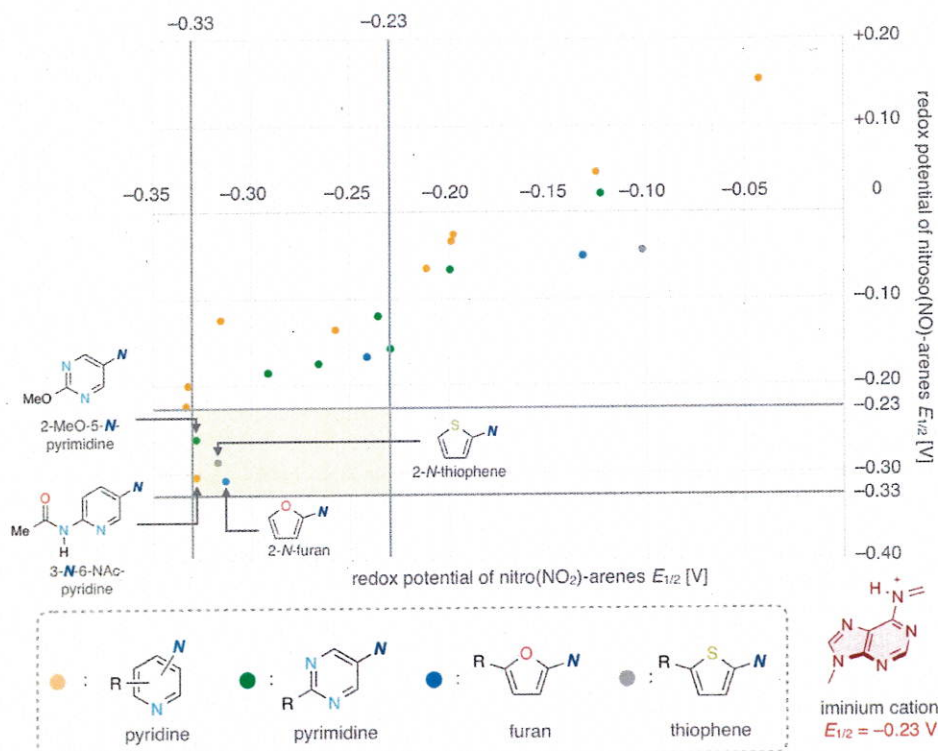
Figure 2-5. Plot of redox potentials of nitro- and nitrosoarenes: CAM-B3LYP/6-31+G(d,p)/SMD (water) at 298 K level of theory. N = NO_2 or NO.

Next, the nitroarenes predicted by the computational study were tested to the N6mA selective DNA modification (Figure 2-6). The reaction using 3-nitro-6-NAc-pyridine showed low conversion due to the insolubility into the water and acetonitrile (19:1) solution. The use of 2-MeO-5-nitropyrimidine resulted in no reaction. Furthermore, the reaction using 2-nitrofuran also showed no reaction. But the reaction color was turned to black after reaction. This result would be caused by side reactions of 2-nitrofuran under photo irradiation conditions. Finally, the corresponding MS signal of the modification product was detected when the DNA modification with 2-nitrothiophene was conducted. Unfortunately, the MS signal was same to the quinuclidine adduct product. However, at least, the same three MS signals were detected in the LC-MS analysis. Therefore, it is anticipated that the 2-nitrothiophene is a first reactive nitroarene probe except for the nitropyridines.
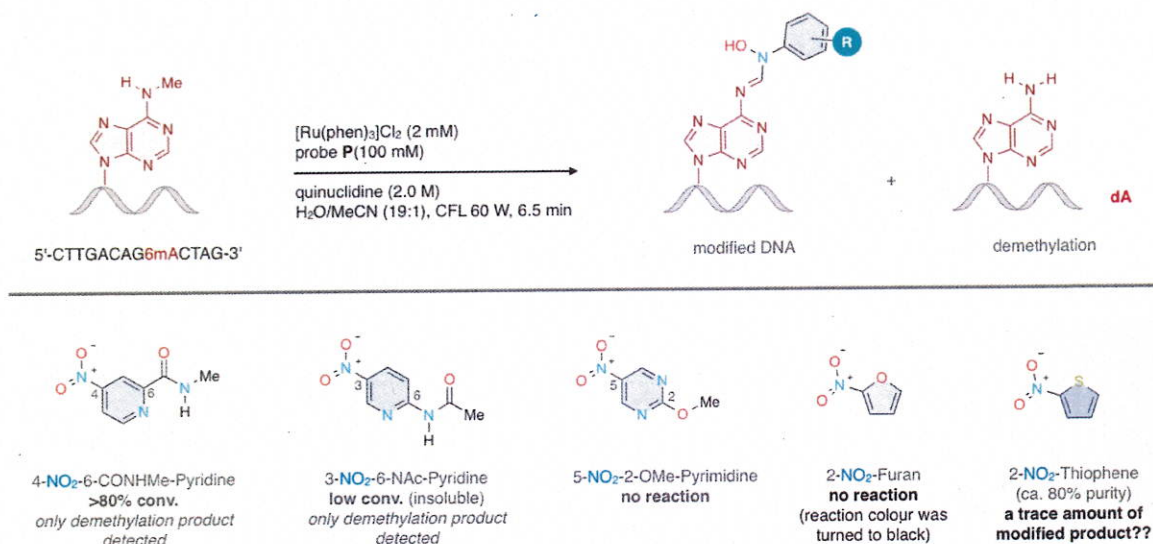

Figure 2-6. Experimental evaluation of predicted probes by DFT calculation for N6mA selective DNA modification.

As a summary, a workflow of computational screening for nitroarenes is shown in Figure 2-7. A first step is an exhaustive screening of more than 40 nitroarenes (Step 1). These nitroarenes should be commercially available or synthesized within one step from the corresponding commercially available chemicals. The nitroarenes were then filtered by whether their redox potentials are higher than that of 3-nitropyridine (−0.33 V) or not. After the first filtering of nitroarenes, the 22 nitroarenes showing higher redox potentials than 3-nitropyridine were found. A

second step is a redox potential calculation of the corresponding the nitrosoarene forms of the 22 nitroarenes. The nitrosoarenes were then filtered by whether their redox potentials are lower than that of the α-amino radical (−0.23V) or not. Finally, the workflow proposed four nitro compounds and one of the four would show the reactivity for the DNA modification. Therefore, it is anticipated that the expansion of nitroarene library for the screening or the addition of other filter requirement for the output should be improve the accuracy.
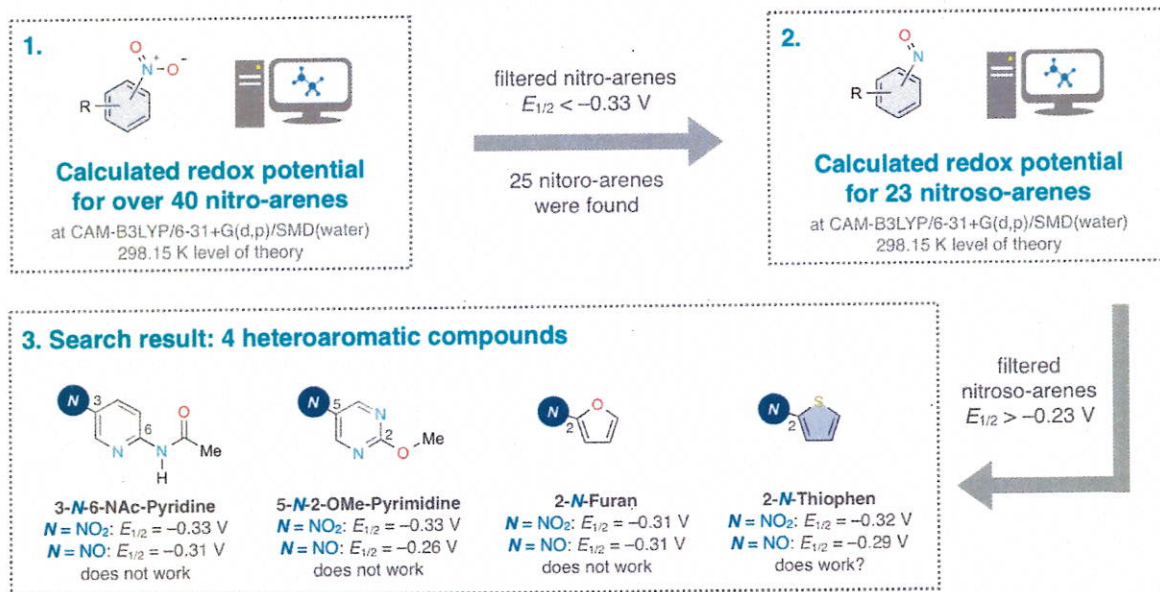

Figure 2-7. Workflow for computational screening of nitroarenes in N6mA selective DNA modification.

Part 3. Investigation of derivatization pathway of *N*-hydroxy formamidine

The N6mA selective DNA modification with nitropyridine and photoredox catalyst gave the product bearing a *N*-hydroxy formamidine moiety. Therefore, the nitropyridine bearing transformative moiety works as a probe for pull-down assay of the modified DNA. The analysis methods such as pull-down assay sometimes requires high stability of target molecules. However, the corresponding modified product was slightly unstable. The corresponding decomposed species (*N*-formylated adenine N6fA) via hydrolysis was detected.
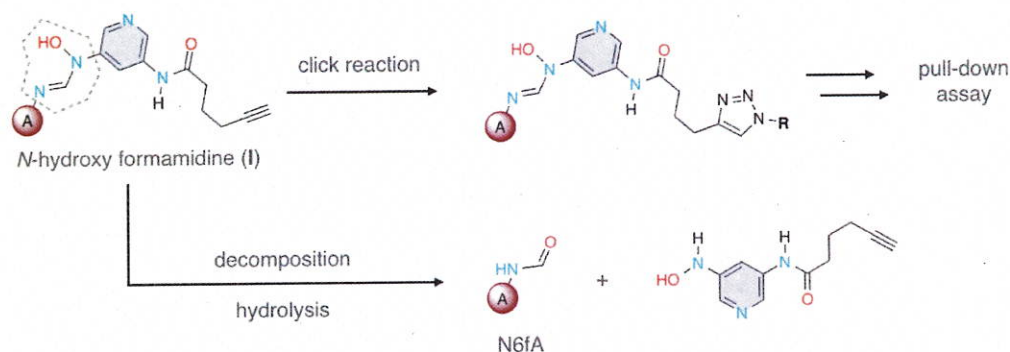

Figure 3-1. Derivatization of modified adenine bearing a *N*-hydroxy formamidine structure and degradation via hydrolysis.

The hydrolysis pathway of the *N*-hydroxy formamidine **I** was calculated to investigate the reaction selectivity between N6fA and adenine A (demethylation product) (Figure 3-2). This calculation was carried out under anionic conditions because the reaction was conducted under high concentration of quinuclidine. The addition of OH⁻ should proceed with reasonable energy barrier (TS1: $\Delta G^{\ddagger} = +10.4$ kcal/mol). And, the stability of the product **II** indicated this reaction should be reversible. Subsequently, the elimination steps generating the 6-formyl adenine or adenine were calculated. The calculation suggested that the elimination of hydroxyamine (TS2: $\Delta G^{\ddagger} = +1.8$ kcal/mol) was significantly faster than the elimination of adenine (TS3: $\Delta G^{\ddagger} = +8.4$ kcal/mol). Whereas, the stability of the products between a pair of 6-formyl-adenine N6fA and 3-hydroxyamine-pyridine **V** and a pair of adenine A and *N*-formyl-3-hydroxyamine-pyridine **VI** was inversed. The pair of **VI** (−12.7 kcal/mol) was thermodynamically more stable than that of **V** (−10.6 kcal/mol). Furthermore, although the reverse reaction from **V** to **III** was lower energetic barrier (+10.2 kcal/mol) compared to that from **VI** to **IV** (+18.4 kcal/mol). Therefore, the nucleophilic

addition of a hydroxy anion (TS1) is a rate-limiting step for the hydrolysis of **I**. The reaction selectivity would kinetically be controlled at first stage. Whereas, the product would finally be converged to the demethylated adenine **VI** by thermodynamic control because the reverse reaction from **V** would be possible.
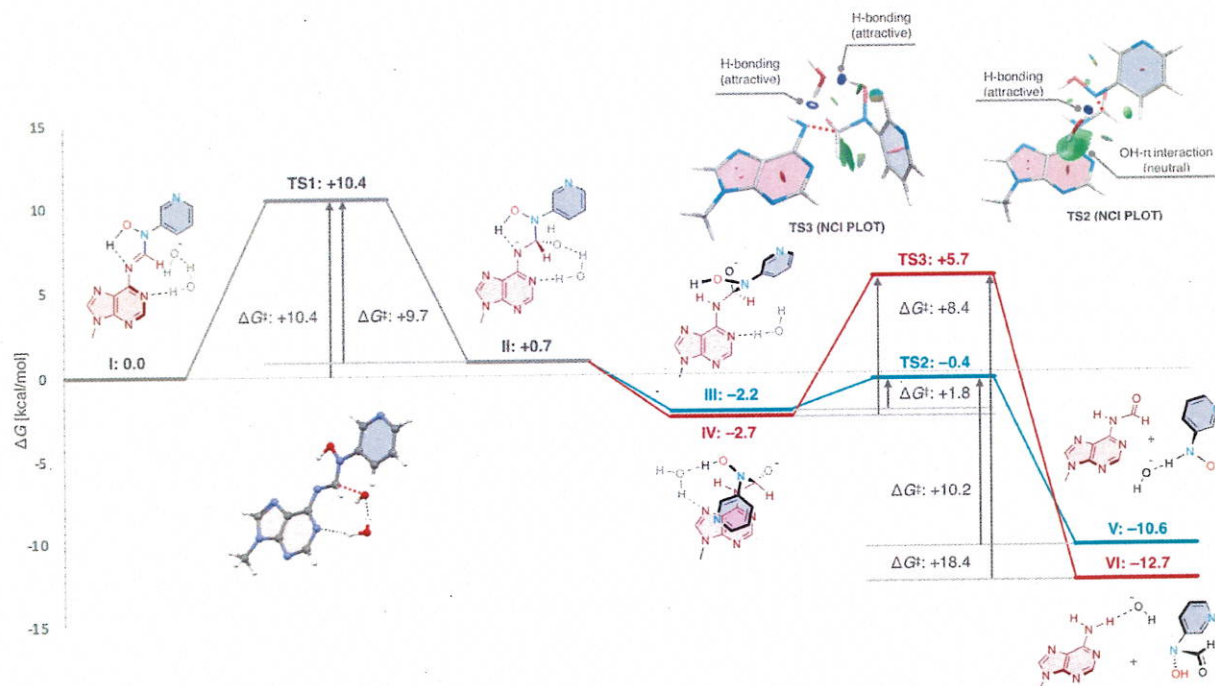

Figure 3-2. Energetic analysis of hydrolysis pathway of *N*-hydroxy formamidine **I** at B3LYP-D3(BJ)/6-311++(2df,2p)/SMD(water)//B3LYP-D3(BJ)/6-31+(d,p)/SMD(water) 298K level of theory.

The various nucleophiles instead of hydroxy anion (OH⁻) for the derivatization of the *N*-hydroxy formamidine **I** were investigated (Figure 3-3). The thermodynamic stability between the adenine bearing a nucleophile **V** (desired) and the demethylate adenine **VI** (undesired) was calculated respectively. The all cases displayed that the pair including adenine **VI** was more stable than that of adenine bearing the nucleophile **V**. Thus, if the derivatization of *N*-hydroxy formamidine using nucleophile would be reversible, the functionalized N6mA would be converted to the the demethylated adenine gradually. Whereas, the difference of the thermodynamic stability between **V** and **VI** was expected relatively small in the DFT calculation when the acyl hydrazine derivative was employed ($\Delta\Delta G$ = +0.5 kcal/mol). Therefore, it would be anticipated that a partial amount of **V** would remain, even if the derivatization of the *N*-hydroxy formamidine by the nucleophile would be reversible. Furthermore, in the case of barbituric acid, the calculated thermodynamic stability of both **V** and **VI** compared to that of the *N*-hydroxy formamidine **I** was high (**V**: ΔG = −16.5 kcal/mol; **VI**: ΔG = −19.2 kcal/mol). This indicated that the reaction of the *N*-hydroxy formamidine **I** using barbituric acid would be irreversible. Consequently, it was expected that the reaction selectivity would kinetically be controlled by the activation energy barriers of TS2 and TS3.
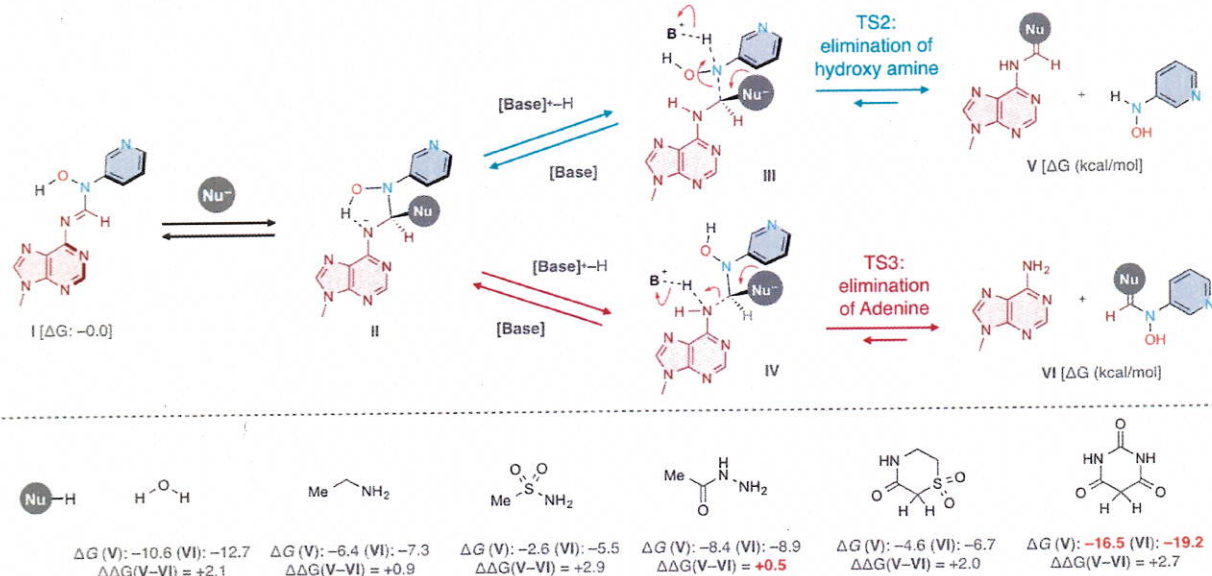
Figure 3-3. Comparison of thermodynamic stability between *N*-hydroxy formamidine **I**, *N*-functionalized adenine **V** and demethylated adenine **VI**.

The further computational study was conducted for mechanistic investigation of the reaction between the *N*-hydroxy formamidine **I** and barbituric acid (Figure 3-4). These calculation results indicated that the activation energy values of TS2 for the *N*-functionalized product **V** was sufficiently lower than that of TS3 for the demethylated product **VI** ($\Delta\Delta G‡$ = +3.0 kcal/mol). to proceed decomposition of the product (**V** and **VI**). Furthermore, the activation energy barriers of the corresponding reversible reactions from **V** or **VI** was high. Therefore, the computation analysis of the nucleophilic substitution of the *N*-hydroxy formamidine **I** by barbituric acid suggested that the selectivity of reaction would be controlled kinetically. Furthermore, acyl hydrazine or barbituric acid would be good nucleophiles for exchanging the functional group on the N-methyl moiety of N6mA to stabilize the *N*-functionalized adenine.
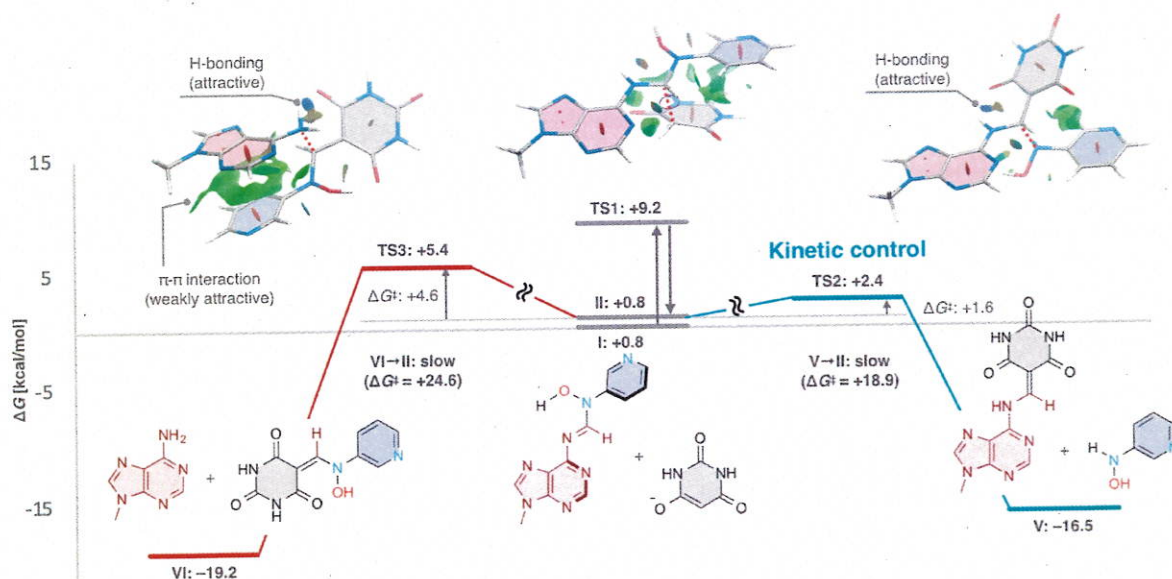

Figure 3-4. Energetic analysis of reaction of *N*-hydroxy formamidine using barbituric acid.

Part 4. Expansion of scope of *N*-methyl selective DNA modification using photoredox catalyst

5-Methylated cytosine (5mdC) is known as a major modified nucleotide in DNA. Furthermore, 4-methylated cytosine (N4mdC) has also been found from the DNA of thermophilic or mesophilic bacteria. Although bisulfite sequencing method converts cytosine, but not 5mdC, to uracil (dU), this method cannot distinguish 5mdC and 4mdC. Recently, sequencing method (4mC-TAB-seq) for DNA including N4mdC and 5mdC combined 5mC selective modification by Tet (ten-eleven translocation) protein and bisulfite sequencing was reported. Whereas, bisulfite sequencing section of N4mC-TAB-seq not only converts dC and modified 5mCd to thymine (dT), but also converts 4mdC to T unselectively. Therefore, it is anticipated that the 4mdC selective DNA modification would have an impact on the efficiency of the DNA sequencing.
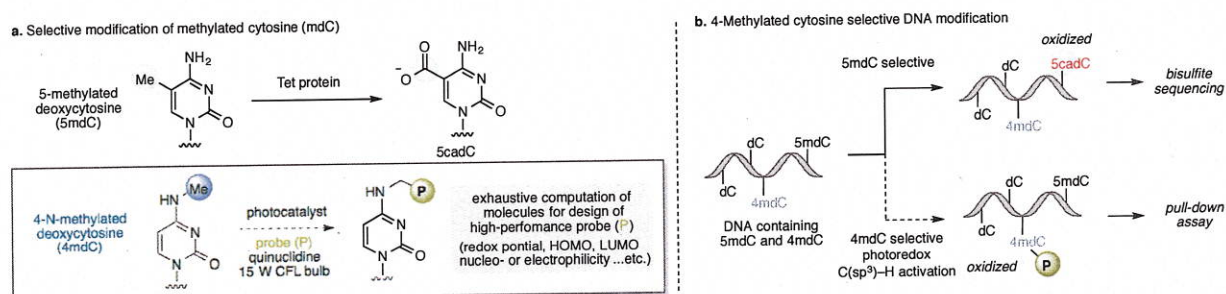

Figure 4-1. Research concepts of N4mC selective DNA modification.

At first, the N4mC selective modification of DNA oligomer contained a N4mC by photocatalyst was conducted (Figure 4-2). In contrast to our expectation, no reaction was occurred under the optimized conditions for the modification of N6mA. Therefore, it suggested that the characters of *N*-methylated
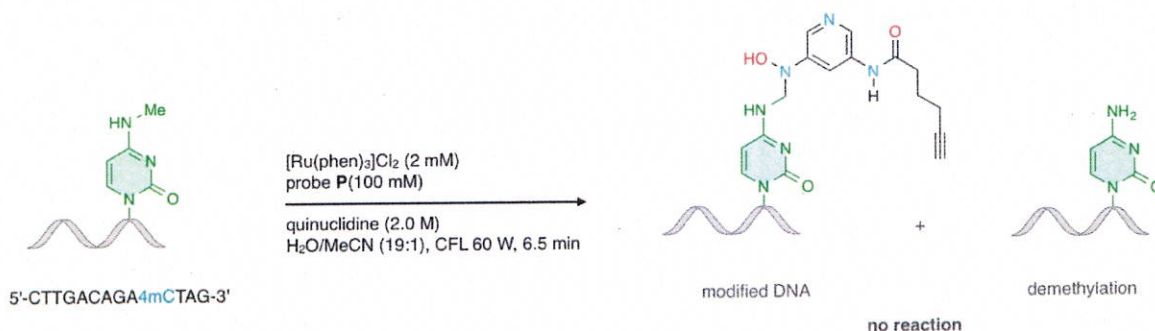
nucleotides would be different respectively.

Figure 4-2. Initial research for N4mC selective DNA modification by photoredox catalyst.

To find the differences between N6mA and N4mC, the charge distribution and spin distribution of α-amino radical intermediates (6mA and 4mC) were estimated (Figure 4-3). The charge distribution at the α-carbon bearing an unpaired electron indicated that these intermediates were nucleophilic radical species (6mA: −0.46; 4mC: −0.46). Furthermore, the spin distribution values displayed that spin of the unpaired electron was localized at the α-carbon. Next, the single occupied molecular orbitals of these radical species suggested that the radical character would be similar to each other because the nitrogen atoms in five membered ring of adenine and the carbonyl moiety of cytosine were not included into their SOMO. However, the SOMO levels of these intermediates indicated that the α-amino radical of adenine would be more nucleophilic than that of cytosine [SOMO(6mA): −5.90 eV; SOMO(4mC): −6.03 eV].
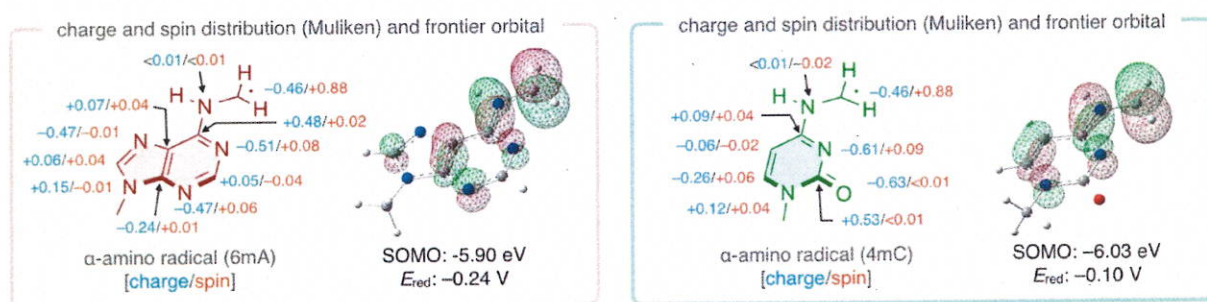

Figure 4-3. Comparison of α-amino radicals of N6mA and N4mC.

Next, the HAT between N4mC and quinuclidine radical cation was calculated to compare with that of N6mA (Figure 4-4). The activation energy of HAT of N4mC was slightly higher than that of N6mA ($\Delta\Delta G^{\ddagger}$ = +1.9 kcal/mol). Furthermore, the BDE of N4mC was also slightly higher than that of N6mA. These indicated that the no reaction in the DNA modification of N4mC would be caused by the slightly strong C–H bond of N-methyl in N4mC Therefore, the long reaction time might be improve the reactivity.
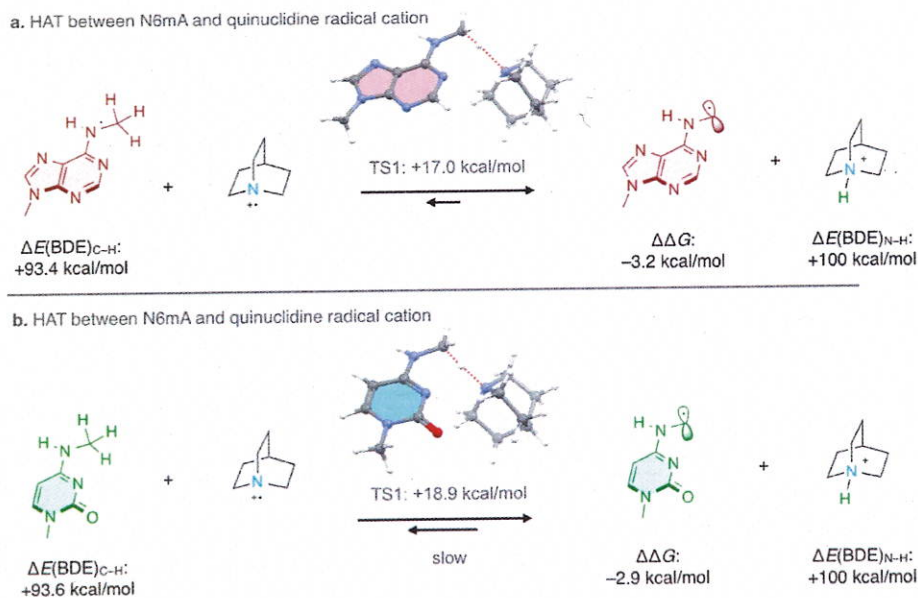
a. HAT between N6mA and quinuclidine radical cation

TS1: +17.0 kcal/mol

$\Delta E(BDE)_{C-H}$: +93.4 kcal/mol

$\Delta\Delta G$: −3.2 kcal/mol

$\Delta E(BDE)_{N-H}$: +100 kcal/mol

b. HAT between N6mA and quinuclidine radical cation

TS1: +18.9 kcal/mol

slow

$\Delta E(BDE)_{C-H}$: +93.6 kcal/mol

$\Delta\Delta G$: −2.9 kcal/mol

$\Delta E(BDE)_{N-H}$: +100 kcal/mol

Figure 4-3. Computational analysis of HAT process and BDE of N6mA and N4mC.

Summary:

In summary, the computational study of the reaction pathway for the *N*-hydroxy formamidine suggested another possible reaction pathway via C–O bond formation between the α-amino radical and nitropyridine. Furthermore, the computational analysis suggested redox potentials of nitro- and nitrosopyridines would involve the reactivity and reaction selectivity. And the acyl hydrazines or barbituric acid would stabilize the N-functionalized adenine for further analysis of the modified DNA.